

# Microscopic Description of Isoscalar Giant Monopole Resonance in $^{48}\text{Ca}$

N. N. Arsenyev<sup>1,\*</sup> and A. P. Severyukhin<sup>1, 2, \*\*</sup>

<sup>1</sup>*Bogoliubov Laboratory of Theoretical Physics,*

*Joint Institute for Nuclear Research, 141980 Dubna, Moscow region, Russia*

<sup>2</sup>*Dubna State University, 141982 Dubna, Moscow region, Russia*

**Abstract** - The properties of the isoscalar giant monopole resonance (ISGMR) for the double magic  $^{48}\text{Ca}$  are analyzed in the framework of a microscopic model based on Skyrme-type interactions. A method for simultaneously taking into account the coupling between one-, two-, and three-phonon terms in the wave functions of  $0^+$  states has been developed. The inclusion of three-phonon configurations leads to a substantial redistribution of the ISGMR strength to lower energy  $0^+$  states and also higher energy tail. Our results demonstrate that the developed approach enables us to describe a gross structure of the ISGMR spreading width.

## 1. INTRODUCTION

The atomic nucleus is a most exceptional quantum many-body system which is characterized by the appearance of various collective excitations. As one of the fundamental excitations in a nucleus, giant resonances are small-amplitude collective vibration modes [1, 2]. Among the giant resonances, a special place is occupied by the isoscalar giant monopole resonances (ISGMR). The ISGMR, the so-called breathing mode, is well localized, which makes it possible to judge from the excitation energies about the incompressibility coefficient of nuclear matter  $K_\infty$  [3, 4]. The incompressibility or the compression modulus is a very fundamental quantity closely connected to the saturation properties of nuclei and to the nucleon–nucleon interaction [4]. This parameter of the nuclear equation of state is important in several physical contexts such as prompt supernova explosions [5, 6], the interiors

---

\* Electronic address: [arsenev@theor.jinr.ru](mailto:arsenev@theor.jinr.ru)

\*\* Electronic address: [sever@theor.jinr.ru](mailto:sever@theor.jinr.ru)

of neutron stars [7, 8], heavy-ion collisions at intermediate and high energies [9, 10].

The extrapolation to nuclear matter and neutron stars requires that the energy of the ISGMR has to be known over a wide range of the mass number  $A$ . In addition to the above, it is also well known that the finite nucleus incompressibility  $K_A$  exhibits a strong mass dependence [4, 11]. Thus, experimental information on the ISGMR from a wide range of nuclei is important. The ISGMR is a well-defined experimental observable, which can be measured precisely through various experimental techniques. The most successful experimental approach [2] to study the ISGMR is inelastic scattering at extreme forward angles because of its selectivity to isoscalar excitations and the dominance of the monopole cross section at angles close to  $0^\circ$ . The ISGMR has been established in heavy nuclei ( $A > 90$ ) where it forms a compact resonance with a Lorentzian shape (see [12], and references therein). It is a general problem in  $A < 90$  nuclei that the isoscalar  $E0$  strength was found to be very fragmented and no longer concentrated in one single peak. Recently, results have become available from the Research Center for Nuclear Physics (RCNP) [13] and the iThemba Laboratory for Accelerator Based Sciences (iThemba LABS) [14] groups for  $^{40,42,44,48}\text{Ca}$  obtained through small angle (including  $0^\circ$ ) inelastic  $\alpha$ -scattering measurements at 386 and 196 MeV, respectively. Both experimental datasets show the fragmentation and splitting of the ISGMR strength distributions. While the iThemba LABS results only cover the range 9.5–25.5 MeV, the studies performed at RCNP presented  $E0$  strengths for significantly larger excitation-energy range 10–31 MeV. For the three nuclei  $^{40,42,44}\text{Ca}$  one observes that the monopole strength distributions from the iThemba LABS study are weaker than those from RCNP, especially at excitation energies around and below the peak of the distribution; see Fig. 6 in [14]. For the case of  $^{48}\text{Ca}$ , in an early  $(\alpha, \alpha')$  study performed by the Texas A&M University Cyclotron Institute (TAMU) group [15] presented the isoscalar  $E0$  strength distribution, which was located between 9.5 and 40 MeV. The iThemba LABS results are in better agreement with previous RCNP datasets, although still weaker than the results from TAMU below the peak of the distribution; see Fig. 6 in [14]. In general, the experimental findings for the  $^{40,42,44,48}\text{Ca}$  isotopes are close. It should be noted that the ISGMR strength distributions were measured using the high energy-resolution capabilities at RCNP, iThemba LABS and TAMU. This allows for the observation of pronounced fine structure. A viable way of understanding the origin and nature of fine structure is to extract the characteristic energy scales from the experimental data and compare them with the most suitable theoretical models.

On the theoretical side, the standard tools for the fine-structure analysis of the ISGMR are random phase approximation (RPA) and its quasiparticle version (QRPA) in the case of open-shell nuclei. It means that the collective  $0^+$  states are constructed in mean-field theory as a coherent superposition of one-particle–one-hole ( $1p1h$ ) excitations [16, 17]. The approach employs the self-consistent mean-field derived from effective nucleon–nucleon interactions that are taken as nonrelativistic two-body Gogny [11, 18–20] and Skyrme [21–31] forces. They are also derived from relativistic Lagrangians, e.g., [32–35]. For spherical nuclei, the extension of the wave function to more complex configurations increases the fragmentation of the initial  $1p1h$  doorway states over many excited states and determines the damping of the giant resonances. As pointed out in [20, 21, 25, 27–29, 31, 33, 36, 37], it allows us to discuss the fine structure of the ISGMR and its damping properties. In Refs. [28, 31] we have shown that the calculations taking into account the phonon–phonon coupling (PPC) describes reasonably well the gross structure of spreading widths of giant monopole resonances in the heavy and superheavy nuclei. In [38] it was shown that the PPC predictions of the fine structure of the ISGMR in  $^{48}\text{Ca}$  are in good agreement with the fine structure which is extracted from experimental data analysis. The PPC calculations use a formalism in which the RPA phonons are treated as boson excitations [39]. The two-phonon amplitudes are defined by the coupling between  $1p1h$  and the two-particle–two-hole ( $2p2h$ ) excitations. These are the basic ingredients of the quasiparticle–phonon model (QPM), but the single-particle (SP) spectrum and the residual interaction are calculated with the Skyrme force; see, for example, [40, 41].

It is remarkable that thanks to experimental advancements, especially at rare ion beam facilities, the investigation of ISGMR of proton- and neutron-rich unstable nuclei has become possible. For exotic nuclei with a large neutron excess, a soft monopole mode may emerge, which brings new insights into the nuclear incompressibility and has become the goals for both experimental and theoretical investigations. For instance, it has been observed experimentally in  $^{11}\text{Li}$  [42] and  $^{68}\text{Ni}$  [43], and is predicted in the neutron-rich Ca [35] and Ni [34], Sn and Pb [26] isotopes. However, for heavy and deformed exotic nuclei, the structure and mechanism of the soft monopole mode are not clear. The soft monopole strength becomes much more fragmented when beyond-mean-field effects are considered [29]. However, most of the available theoretical calculations are based on the QRPA or beyond QRPA which is limited to interaction with the  $2p2h$  configurations.

In the present paper, we propose an extension of our PPC approach taking into account the coupling between one-, two-, and three-phonon terms in the wave functions of excited  $0^+$  states. As an application of the method we present results for the change in the monopole strength function profile caused by the  $3p3h$  fragmentation and analyze its impact on the characteristics of the ISGMR in the case of double closed-shell nucleus  $^{48}\text{Ca}$ . The recent ISGMR strength distribution measurements through small angle inelastic  $\alpha$ -scattering give an opportunity to compare our results and the experimental data [13, 14].

## 2. BASIC ELEMENTS OF THE MICROSCOPIC APPROACH

The starting point of our microscopic approach consists in the Hartree–Fock (HF) calculation of the ground state based on the Skyrme energy density functional (EDF) [17, 44]. Spherical symmetry is imposed on the HF wave functions. The continuous part of the SP spectrum is discretized by diagonalizing the HF Hamiltonian on a harmonic oscillator basis [18]. The residual particle–hole interaction is obtained as the second derivative of the energy density functional with respect to the particle density. By means of the standard procedure [24] we obtain the familiar RPA equations in the  $1p1h$  configuration space. The eigenvalues of the RPA equations are found numerically as the roots of a relatively simple secular equation within the finite rank separable approximation (FRSA) [45, 46]. Making use of the FRSA for the residual interaction enables us to perform RPA calculations in very large configurational spaces. In particular, the cutoff of the discretized continuous part of the SP spectra is at the energy of 100 MeV. This is sufficient to exhaust practically all the energy-weighted sum rules (EWSR) within the RPA. It is worth mentioning that the so-called FRSA has been successfully used to study the electromagnetic transitions between excited states [41, 47] and the ISGMR strength distribution within and beyond the QRPA [28, 31, 38].

Using the basic QPM ideas in the simplest case of the configuration mixing [39, 48], we construct the wave functions from a linear combination of one-, two-, and three-RPA

phonons [49–51],

$$\Psi_\nu(JM) = \left( \sum_i R_i(J\nu) Q_{JMi}^+ + \sum_{\lambda_1 i_1 \lambda_2 i_2} P_{\lambda_2 i_2}^{\lambda_1 i_1}(J\nu) [Q_{\lambda_1 \mu_1 i_1}^+ Q_{\lambda_2 \mu_2 i_2}^+]_{JM} \right. \\ \left. + \sum_{\lambda_1 i_1 \lambda_2 i_2 \lambda_3 i_3 J'} T_{J' \lambda_3 i_3}^{\lambda_1 i_1 \lambda_2 i_2}(J\nu) [[Q_{\lambda_1 \mu_1 i_1}^+ Q_{\lambda_2 \mu_2 i_2}^+]_{J'} Q_{\lambda_3 \mu_3 i_3}^+]_{JM} \right) |0\rangle, \quad (1)$$

in which  $\lambda$  denotes the total angular momentum,  $\mu$  is its  $z$ -projection in the laboratory system and sequential number  $i$ ; the  $[\dots]_{JM}$  stands for angular momentum coupling. The ground state is the RPA phonon vacuum  $|0\rangle$ . The wave functions of the one-RPA phonon excited states, having energy  $\omega_{\lambda i}$ , given by  $Q_{\lambda \mu i}^+ |0\rangle$  as a superposition of the  $1p1h$  configurations. The normalization condition for the wave functions (1) yields

$$\sum_i [R_i(J\nu)]^2 + 2 \sum_{\lambda_1 i_1 \lambda_2 i_2} [P_{\lambda_2 i_2}^{\lambda_1 i_1}(J\nu)]^2 + 6 \sum_{\lambda_1 i_1 \lambda_2 i_2 \lambda_3 i_3 J'} [T_{J' \lambda_3 i_3}^{\lambda_1 i_1 \lambda_2 i_2}(J\nu)]^2 = 1. \quad (2)$$

The variational principle leads to a set of linear equations for the unknown amplitudes  $R_i(J\nu)$ ,  $P_{\lambda_2 i_2}^{\lambda_1 i_1}(J\nu)$  and  $T_{J' \lambda_3 i_3}^{\lambda_1 i_1 \lambda_2 i_2}(J\nu)$  (see details in [39, 48–50]):

$$R_i(J\nu) (\omega_{Ji} - E_\nu) + \sum_{\lambda_1 i_1 \lambda_2 i_2} P_{\lambda_2 i_2}^{\lambda_1 i_1}(J\nu) U_{\lambda_2 i_2}^{\lambda_1 i_1}(Ji) = 0, \quad (3)$$

$$P_{\lambda_2 i_2}^{\lambda_1 i_1}(J\nu) (\omega_{\lambda_1 i_1} + \omega_{\lambda_2 i_2} - E_\nu) + 3 \sum_{\lambda'_1 i'_1 \lambda'_2 i'_2} T_{\lambda_1 \lambda_2 i_2}^{\lambda'_1 i'_1 \lambda'_2 i'_2}(J\nu) U_{\lambda'_2 i'_2}^{\lambda'_1 i'_1}(\lambda_1 i_1) \\ + \frac{1}{2} \sum_{i'} U_{\lambda_2 i_2}^{\lambda_1 i_1}(Ji') R_{i'}(J\nu) = 0, \quad (4)$$

$$T_{J' \lambda'_3 i'_3}^{\lambda'_1 i'_1 \lambda'_2 i'_2}(J\nu) (\omega_{\lambda'_1 i'_1} + \omega_{\lambda'_2 i'_2} + \omega_{\lambda'_3 i'_3} - E_\nu) + \sum_i P_{\lambda'_3 i'_3}^{J' i}(J\nu) U_{\lambda'_2 i'_2}^{\lambda'_1 i'_1}(J'i) = 0. \quad (5)$$

The rank of the set of linear Eqs. (3), (4) and (5) is equal to the number of one-, two-, and three-phonon configurations included in the wave function (1). To resolve this set it is required to compute the coupling matrix elements

$$U_{\lambda_2 i_2}^{\lambda_1 i_1}(Ji) = \langle 0 | Q_{Ji} \mathcal{H} [Q_{\lambda_1 i_1}^+ Q_{\lambda_2 i_2}^+]_J | 0 \rangle \quad (6)$$

between one- and two-phonon configurations (see details in [40]). Evidently, the nonzero matrix elements  $U_{\lambda_2 i_2}^{\lambda_1 i_1}(Ji)$  result in the inclusion of the PPC effects. Equations (3), (4) and (5) have the same form as the QPM equations [50]. However, the SP spectrum and the parameters of the residual interaction are calculated with the chosen Skyrme forces, without any further adjustments. We consider widely used SLy5 EDF [52] which is adjusted to

**Table 1.** Energies and  $B(E\lambda)$  values for the transitions to the ground states in  $^{48}\text{Ca}$ ; experimental data

$\lambda_1^\pi$	are taken from [53]			
	Energy,		$B(E\lambda; \lambda_1^\pi \rightarrow 0_{\text{g.s.}}^+)$ ,	
	MeV		W.u.	
	Expt.	Theory	Expt.	Theory
$2_1^+$	3.832	3.19	$1.84_{-0.14}^{+0.17}$	1.3
$3_1^-$	4.507	4.47	$8.4_{-3.5}^{+4.3}$	4.1
$4_1^+$	4.503	3.51		2.1
$5_1^-$	5.729	4.52		8.7

reproduce the nuclear matter properties, as well as nuclear charge radii, binding energies of doubly-magic nuclei [44].

The excitation operator of the ISGMR is defined as

$$\hat{M}_{\lambda=0} = \sum_{i=1}^A r_i^2. \quad (7)$$

The wave functions (1) allow us to determine the transition probabilities  $\left| \langle 0_\nu^+ | \hat{M}_{\lambda=0} | 0_{\text{g.s.}}^+ \rangle \right|^2$ . To construct the wave functions (1) of the excited  $0^+$  states, in the actual calculations (PPC3), we take into account all two- and three-phonon configurations below 30 MeV that are built from the phonons with different multipoles  $\lambda^\pi = 0^+, 1^-, 2^+, 3^-, 4^+$ , and  $5^-$  coupled to  $J^\pi = 0^+$ . If we omit the three-phonon configurations, then this calculation is hereafter called PPC2.

Another important aspect in the RPA basic is related to the description of the low-lying states. The energies and reduced transition probabilities of the  $[2_1^+]_{\text{RPA}}$ ,  $[3_1^-]_{\text{RPA}}$ ,  $[4_1^+]_{\text{RPA}}$ , and  $[5_1^-]_{\text{RPA}}$  states are presented in Table 1. The RPA results obtained within the SLy5 EDF are compared with the experimental data [53]. As one can see, the overall agreement of the energies and  $B(E\lambda)$  values with the data looks reasonable. It is remarkable that the PPC3 plays a minor role, for example, in the  $2_1^+$  state's description [51, 54]. The crucial contribution to the wave function comes from the neutron configuration  $\{1f_{\frac{7}{2}}, 2p_{\frac{3}{2}}\}$ .

### 3. THE RESULTS OF MICROSCOPIC CALCULATIONS

As a first step in testing our approach we consider the  $E0$  strength distribution in the ISGMR energy region. Using the excitation energies  $E_\nu$  and the transition probabilities  $\left| \langle 0_\nu^+ | \hat{M}_{\lambda=0} | 0_{\text{g.s.}}^+ \rangle \right|^2$ , the isoscalar monopole strength distribution is averaged out by a Lorentzian distribution with a width of 1.0 MeV as follows:

$$S(\omega) = \sum_\nu \left| \langle 0_\nu^+ | \hat{M}_{\lambda=0} | 0_{\text{g.s.}}^+ \rangle \right|^2 \frac{1}{2\pi} \frac{\Delta}{(\omega - E_\nu)^2 + \Delta^2/4}. \quad (8)$$

The ISGMR strength distribution up to 30 MeV is displayed in Fig. 1. Unlike the ISGMR for the heavy nuclei ( $A > 90$ ) [12] which concentrates in a single collective peak, the strength function of ISGMR for  $^{48}\text{Ca}$  is fragmented. Both experimental [13, 14] and theoretical results showed the fragmentation and splitting of the ISGMR strength. Let us look at the calculated strength distributions in more detail. There is the low-energy part below 10 MeV, the main peak in the ISGMR region (10.0–25.5 MeV) and the high-energy tail above 25.5 MeV. The results of the RPA calculation are shown in Fig. 1. According to RPA calculations the lowest  $0^+$  state appears above 14 MeV. The ISGMR strength in the energy range 10.0–25.5 MeV exhausts 92.7% of the total monopole strength which we obtained below 30 MeV. The RPA strength distribution is practically concentrated on three states at 18.3, 19.4, and 22.6 MeV, which exhausts 89.4% of the EWSR,  $2\hbar^2 A \langle r^2 \rangle / m$  [55], or about 79.3% of the total monopole strength. The rest of the monopole strength lies in the high-energy region.

The coupling between the one-, and two-phonon configurations (dashed curve in Fig. 1), PPC2, yields a noticeable redistribution of the ISGMR strength in comparison with the RPA results (dotted curve in Fig. 1). Comparing the RPA results, we see that a single peak appears at 17.4 MeV, which exhausts 13.3% of the EWSR value. The two-phonon coupling produces a shift of order 0.6% and 8.6% of the total monopole strength from the ISGMR region to the low- and high-energy regions, respectively. We recall that the importance of the complex configurations for the interpretation of basic peculiarities of the ISGMR strength distribution of  $^{48}\text{Ca}$  was already qualitatively discussed in the framework of the microscopic calculations including  $1p1h$  coupled to phonon configurations [37]. Our calculations give the same tendency.

The extension of the configuration space to the three-phonon configurations (solid curve in Fig. 1), PPC3, also has a strong effect on the ISGMR strength distribution in comparison

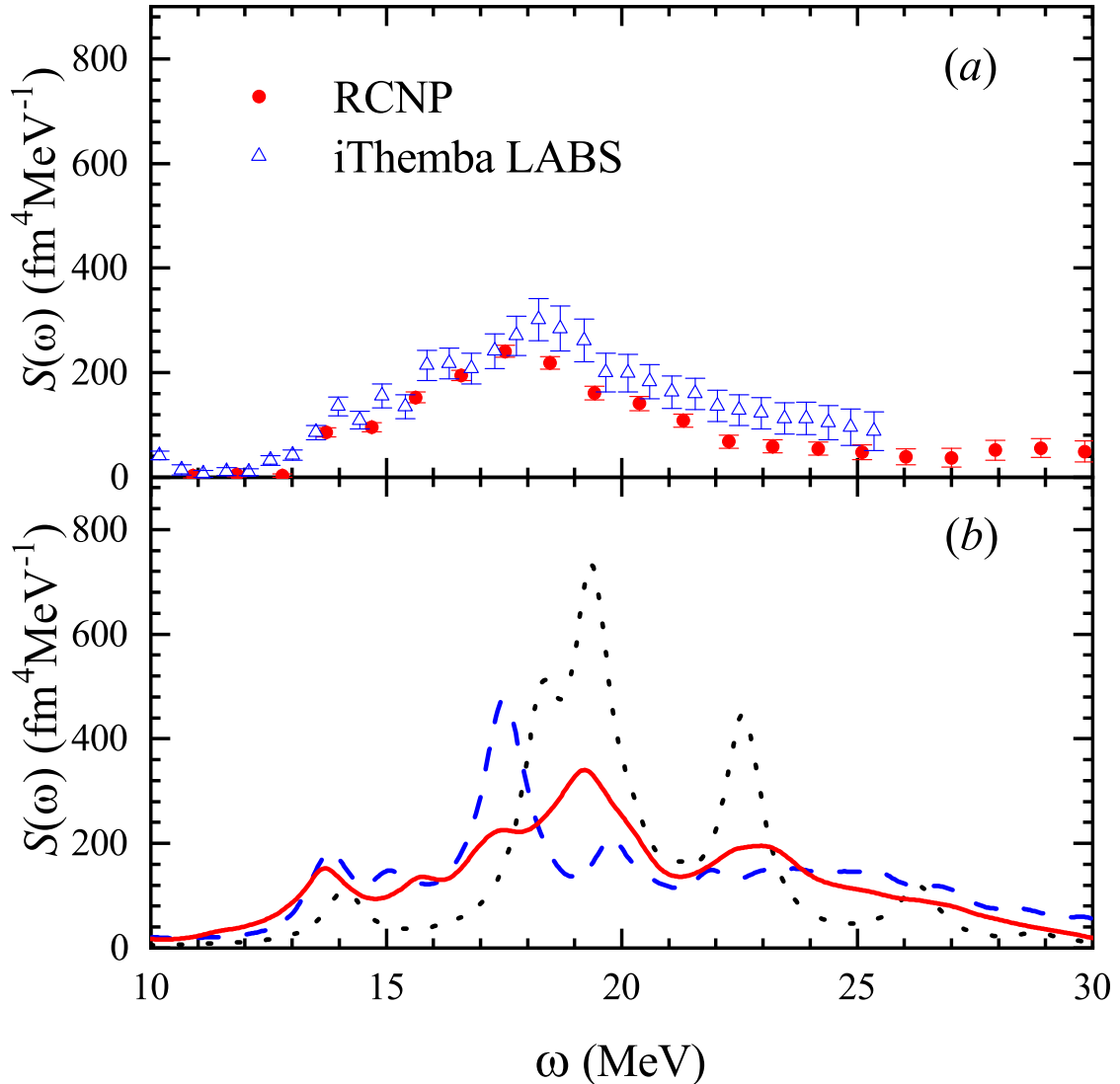


**Figure 1.** Panel (a) experimental ISGMR strength distributions. Experimental data are taken from [13, 14]. Panel (b). Comparison of the results obtained by means of the microscopic calculations. The dotted, dashed and solid curves correspond to the RPA, PPC2 and PPC3 calculations, respectively. The smoothing parameter 1 MeV is used for the strength distribution described by the Lorentzian function.

with the PPC2 results (dashed curve in Fig. 1). In particular, the PPC3 effect leads to a shift of the main peak by 1800 keV towards higher energies. Moreover, the three-phonon coupling induces a shift of order 0.6% of the total monopole strength from the ISGMR region to the lower energy region ( $E_x < 10.0$  MeV). At the same time, the PPC3 effect pumps about 5.8% of the total monopole strength from the high-energy tail of the ISGMR to the resonance region (10.0–25.5 MeV). As a result, our analysis showed that the  $2p2h$  and  $3p3h$  fragmentations shift about 1.2% (2.8%) of the total monopole strength into the lower

**Table 2.** Moment ratios of the  $E0$  strength distributions calculated over the excitation-energy range

10.0–25.5 MeV; experimental data are taken from [14]			
	$m_1/m_0$ , MeV	$\sqrt{m_1/m_{-1}}$ , MeV	$\sqrt{m_3/m_1}$ , MeV
RPA	19.8	19.6	20.1
PPC2	18.9	18.5	19.8
PPC3	19.1	18.8	19.9
RCNP	$18.01 \pm 0.10$	$17.75 \pm 0.10$	$18.78 \pm 0.13$
iThemba LABS	$18.40 \pm 0.13$	$18.09 \pm 0.12$	$19.29 \pm 0.15$
TAMU	$17.52 \pm 0.10$	$17.11 \pm 0.10$	$18.69 \pm 0.05$

energy region ( $E_x < 10.0$  MeV) and the higher energy region ( $E_x > 25.5$  MeV), respectively. As can be seen from Fig. 1, the general shapes of the ISGMR obtained in the PPC3 are somewhat close to those observed in the RCNP and iThemba LABS experiments. This demonstrates the improvement of the PPC3 description in comparison with RPA and also PPC2. We conclude that the main mechanisms of the ISGMR formation in  $^{48}\text{Ca}$  can be taken into account correctly and consistently in the PPC approach.

In order to discuss the various integral characteristics, we introduce the energy-weighted moments  $m_k$

$$m_k = \sum_{\nu} (E_{\nu})^k \left| \langle 0_{\nu}^+ | \hat{M}_{\lambda=0} | 0_{\text{g.s.}}^+ \rangle \right|^2. \quad (9)$$

These values are useful in estimating the resonance centroid and also in checking numerical calculations. Let us examine the various moment ratios of the  $E0$  strength distribution. The calculated ratios are given in Table 2. They are compared with experimental data [14]. In [14], the experimental datasets of the three groups are discussed. The integral characteristics of  $E0$  strength function have been obtained in the energy region of 10.0–25.5 MeV. It can be seen, that the PPC3 induces a 700-keV downward shift of the ISGMR centroid energy  $E_c = m_1/m_0$  compared to the RPA; see Table 2. In general, these results indicate that the PPC3 predictions lead to a better agreement (compared to RPA) with these known experimental values. To test futher the validity of our microscopic approach we compare the calculated spreading width  $\Gamma = 2.35 \sqrt{m_2/m_0 - (m_1/m_0)^2}$  with the experimental data available for  $^{48}\text{Ca}$ . We obtained that the PPC3 coupling increases the ISGMR width from 5.1 to

7.8 MeV. The experimental ISGMR width is  $6.68^{+0.31}_{-0.36}$  MeV [15], but we note that in the presented rms width was obtained in the energy region 9.5–40.0 MeV. In [56], the ISGMR width for  $^{48}\text{Ca}$  is 7.78 MeV obtained through small angle inelastic  $\alpha$ -scattering measurements at 200 MeV. The ISGMR width was extracted by applying a Lorentzian curve in the excitation energy region of 12.0–24.0 MeV. One can see more and less good agreement between the calculated and available experimental data.

#### 4. CONCLUSIONS

Beginning with the mean-field calculations with the Skyrme force SLy5 the properties of the spectrum of  $0^+$  excitations of  $^{48}\text{Ca}$  were studied within the FRSA model, including the effects of the phonon-phonon coupling. The inclusion of the coupling between one-, two-, and three-phonon terms in the wave functions of excited  $0^+$  states leads to a redistribution of the strength of the ISGMR. A part of the main peak strength is fragmented in the low-energy states and the main peak itself is shifted downwards. The coupling with  $3p3h$  excitations shifts about 1% of the total monopole strength into the lower energy region ( $E_x < 10.0$  MeV) and 3% into the higher energy region ( $E_x > 25.5$  MeV). The crucial contribution in the wave-function structure of the low-lying  $0^+$  states ( $E_x < 10.0$  MeV) comes from the two-phonon configurations. It is shown that the  $2p2h$  and  $3p3h$  fragmentations lead to an increase in the ISGMR width. Our results are in reasonable agreement with the recently experimental data for  $^{48}\text{Ca}$ .

#### ACKNOWLEDGMENTS

Very fruitful discussions with Sunday Olorunfunmi, and Armand Bahini are gratefully acknowledged. We thank Iyabo Usman for providing insights and numerical data for the experimental monopole strength in  $^{48}\text{Ca}$ . A.N.N. acknowledges support from the Russian Science Foundation (Grant No. RSF-21-12-00061). The work of A.P.S. was supported by the National Research Foundation of South Africa (Grant No. 129603).

## REFERENCES

---

1. P. F. Bortignon, A. Bracco, and R. A. Broglia, *Giant Resonances: Nuclear Structure at Finite Temperature* (Harwood Academic, Amsterdam, 1998).
2. M. N. Harakeh and A. van der Woude, *Giant Resonances: Fundamental High-Frequency Modes of Nuclear Excitation* (Oxford University Press, Oxford, 2001).
3. O. Bohigas, A. M. Lane, and J. Martorell, Phys. Rep. **51**, 267 (1979).
4. J. P. Blaizot, Phys. Rep. **64**, 171 (1980).
5. E. Baron, J. Cooperstein, and S. Kahana, Phys. Rev. Lett. **55**, 126 (1985).
6. H. A. Bethe, Rev. Mod. Phys. **62**, 801 (1990).
7. N. K. Glendenning, Phys. Rev. Lett. **57**, 1120 (1986).
8. J. M. Lattimer and M. Prakash, Astrophys. J. **550**, 426 (2001).
9. H. Stöcker and W. Greiner, Phys. Rep. **137**, 277 (1986).
10. V. Baran, M. Colonna, V. Greco, and M. Di Toro, Phys. Rep. **410**, 335 (2005).
11. J. P. Blaizot, D. Gogny, and B. Grammaticos, Nucl. Phys. A **265**, 315 (1976).
12. U. Garg and G. Colò, Prog. Part. Nucl. Phys. **101**, 55 (2018).
13. K. B. Howard, U. Garg, M. Itoh, H. Akimune, S. Bagchi, T. Doi, Y. Fujikawa, M. Fujiwara, T. Furuno, M. N. Harakeh, Y. Hijikata, K. Inaba, S. Ishida, N. Kalantar-Nayestanaki, T. Kawabata, S. Kawashima, et al., Phys. Lett. B **801**, 135185 (2020).
14. S. D. Olorunfunmi, R. Neveling, J. Carter, P. von Neumann-Cosel, I. T. Usman, P. Adsley, A. Bahini, L. P. L. Baloyi, J. W. Brümmer, L. M. Donaldson, H. Jivan, N. Y. Kheswa, K. C. W. Li, D. J. Marín-Lámbarri, P. T. Molema, C. S. Moodley, et al., Phys. Rev. C **105**, 054319 (2022).
15. Y.-W. Lui, D. H. Youngblood, S. Shlomo, X. Chen, Y. Tokimoto, Krishichayan, M. Anders, and J. Button, Phys. Rev. C **83**, 044327 (2011).
16. D. J. Rowe, *Nuclear Collective Motion* (Methuen, London, 1970).
17. P. Ring and P. Schuck, *The Nuclear Many Body Problem* (Springer, Berlin, 1980).
18. J. P. Blaizot and D. Gogny, Nucl. Phys. A **284**, 429 (1977).
19. S. Péru, J. F. Berger, and P. F. Bortignon, Eur. Phys. J. A **26**, 25 (2005).

20. D. Gambacurta, M. Grasso, V. De Donno, G. Co', and F. Catara, Phys. Rev. C **86**, 021304(R) (2012).
21. S. Adachi and S. Yoshida, Nucl. Phys. A **306**, 53 (1978).
22. Nguyen Van Giai and H. Sagawa, Nucl. Phys. A **371**, 1 (1981).
23. B. K. Agrawal and S. Shlomo, Phys. Rev. C **70**, 014308 (2004).
24. J. Terasaki, J. Engel, M. Bender, J. Dobaczewski, W. Nazarewicz, and M. Stoitsov, Phys. Rev. C **71**, 034310 (2005).
25. V. Tselyaev, J. Speth, S. Krewald, E. Litvinova, S. Kamerdzhev, N. Lyutorovich, A. Avdeenkov, and F. Grümmer, Phys. Rev. C **79**, 034309 (2009).
26. E. Khan, N. Paar, D. Vretenar, L.-G. Cao, H. Sagawa, and G. Colò, Phys. Rev. C **87**, 064311 (2013).
27. X. Roca-Maza, Y. F. Niu, G. Colò, and P. F. Bortignon, J. Phys. G: Nucl. Part. Phys. **44**, 044001 (2017).
28. A. P. Severyukhin, S. Åberg, N. N. Arsenyev, and R. G. Nazmitdinov, Phys. Rev. C **95**, 061305(R) (2017); **97**, 059802 (2018).
29. D. Gambacurta, M. Grasso, and O. Sorlin, Phys. Rev. C **100**, 014317 (2019).
30. G. Colò, D. Gambacurta, W. Kleinig, J. Kvasil, V. Nesterenko, and A. Pastore, Phys. Lett. B **811**, 135940 (2020).
31. N. N. Arsenyev and A. P. Severyukhin, Universe **7**, 145 (2021).
32. D. Vretenar, T. Nikšić, and P. Ring, Phys. Rev. C **68**, 024310 (2003).
33. E. Litvinova, P. Ring, and V. Tselyaev, Phys. Rev. C **75**, 064308 (2007).
34. J. Piekarewicz, Phys. Rev. C **91**, 014303 (2015).
35. J. Piekarewicz, Phys. Rev. C **96**, 044314 (2017).
36. S. Drozdź, S. Nishizaki, J. Speth, and J. Wambach, Phys. Rep. **197**, 1 (1990).
37. S. Kamerdzhev, J. Speth, and G. Tertychny, Phys. Rep. **393**, 1 (2004).
38. S. D. Olorunfunmi, I. T. Usman, J. Carter, L. Pellegrini, P. T. Molema, E. Sideras-Haddad, R. Neveling, F. D. Smit, P. Adsley, L. M. Donaldson, L. Pellegrini, G. F. Steyn, P. von Neumann-Cosel, N. Pietralla, N. N. Arsenyev, P. Papka, et al., J. Phys.: Conf. Ser. **1643**, 012154 (2020).
39. V. G. Soloviev, *Theory of Atomic Nuclei: Quasiparticles and Phonons* (Institute of Physics, Bristol and Philadelphia, 1992).
40. A. P. Severyukhin, V. V. Voronov, and Nguyen Van Giai, Eur. Phys. J. A **22**, 397 (2004).

41. A. P. Severyukhin, N. N. Arsenyev, and N. Pietralla, Phys. Rev. C **86**, 024311 (2012).
42. S. A. Fayans, S. N. Ershov, and E. F. Svinareva, Phys. Lett. B **292**, 239 (1992).
43. M. Vandebruck, J. Gibelin, E. Khan, N. L. Achouri, H. Baba, D. Beaumel, Y. Blumenfeld, M. Caamaño, L. Cáceres, G. Colò, F. Delaunay, B. Fernandez-Dominguez, U. Garg, G. F. Grinyer, M. N. Harakeh, N. Kalantar-Nayestanaki, et al., Phys. Rev. Lett. **113**, 032504 (2014).
44. M. Bender, P.-H. Heenen, and P.-G. Reinhard, Rev. Mod. Phys. **75**, 121 (2003).
45. Nguyen Van Giai, Ch. Stoyanov, and V. V. Voronov, Phys. Rev. C **57**, 1204 (1998).
46. A. P. Severyukhin, V. V. Voronov, and Nguyen Van Giai, Phys. Rev. C **77**, 024322 (2008).
47. A. P. Severyukhin, N. N. Arsenyev, I. N. Borzov, E. O. Sushenok, D. Testov, and D. Verney, Phys. Rev. C **101**, 054309 (2020).
48. N. Lo Iudice, V. Yu. Ponomarev, Ch. Stoyanov, A. V. Sushkov, and V. V. Voronov, J. Phys. G: Nucl. Part. Phys. **39**, 043101 (2012).
49. M. Grinberg and Ch. Stoyanov, Nucl. Phys. A **573**, 231 (1994).
50. M. Grinberg, Ch. Stoyanov, and N. Tsoneva, Fiz. Elem. Chastits At. Yadra **29**, 1456 (1998) [Phys. Part. Nucl. **29**, 606 (1998)].
51. A. P. Severyukhin, N. N. Arsenyev, and N. Pietralla, Phys. Rev. C **104**, 024310 (2021).
52. E. Chabanat, P. Bonche, P. Haensel, J. Meyer, and R. Schaeffer, Nucl. Phys. A **635**, 231 (1998); **643**, 441(E) (1998).
53. J. Chen, Nucl. Data Sheets **179**, 1 (2022).
54. N. N. Arsenyev, A. P. Severyukhin, V. V. Voronov, and Nguyen Van Giai, Phys. Rev. C **95**, 054312 (2017).
55. J. Martorell, O. Bohigas, S. Fallieros, and A. M. Lane, Phys. Lett. B **60**, 313 (1976).
56. S. D. Olorunfunmi, PhD thesis (University of the Witwatersrand, 2020).